

Origination of the modern-style diversity gradient 15 million years ago

<https://doi.org/10.1038/s41586-023-05712-6>

Isabel S. Fenton¹, Tracy Aze², Alexander Farnsworth^{3,4}, Paul Valdes³ & Erin E. Saupe¹✉

Received: 4 August 2022

Accepted: 6 January 2023

Published online: 15 February 2023

 Check for updates

The latitudinal diversity gradient (LDG) is a prevalent feature of modern ecosystems across diverse clades^{1–4}. Recognized for well over a century, the causal mechanisms for LDGs remain disputed, in part because numerous putative drivers simultaneously covary with latitude^{1,3,5}. The past provides the opportunity to disentangle LDG mechanisms because the relationships among biodiversity, latitude and possible causal factors have varied over time^{6–9}. Here we quantify the emergence of the LDG in planktonic foraminifera at high spatiotemporal resolution over the past 40 million years, finding that a modern-style gradient arose only 15 million years ago. Spatial and temporal models suggest that LDGs for planktonic foraminifera may be controlled by the physical structure of the water column. Steepening of the latitudinal temperature gradient over 15 million years ago, associated with an increased vertical temperature gradient at low latitudes, may have enhanced niche partitioning and provided more opportunities for speciation at low latitudes. Supporting this hypothesis, we find that higher rates of low-latitude speciation steepened the diversity gradient, consistent with spatiotemporal patterns of depth partitioning by planktonic foraminifera. Extirpation of species from high latitudes also strengthened the LDG, but this effect tended to be weaker than speciation. Our results provide a step change in understanding the evolution of marine LDGs over long timescales.

The spatial structure of Earth's biodiversity has the potential to provide important insight on evolutionary drivers. Today, species richness peaks at low latitudes in both marine^{10–12} and terrestrial^{1,4} systems across diverse taxonomic groups, referred to as the LDG. Although first documented over 200 years ago, the causal mechanisms responsible for elevated low-latitude richness are still disputed^{1,3,4,13}.

LDGs derive from differential rates of speciation, extinction, local extirpation, and dispersal^{14,15}, which themselves may be controlled by the dynamics of climate^{14,16–19}, biotic interactions^{20–23}, energy or primary production^{24,25}, or available surface area²⁶. Identifying which of these factors are key controls on rates of speciation, extinction, extirpation and dispersal is difficult because most are collinear with each other today⁵. However, the relationship between latitude and these hypothesized drivers has not been constant over Earth history, and thus intervals of the geological past can provide insight on how biodiversity is generated and maintained^{6,7,9}.

In marine systems, previous work has suggested that diversity gradients were present for tens of millions of years but varied in strength and shape^{4,6–9}. However, limited fossil data have prevented detailed examination of the emergence of modern-day LDGs for more than short temporal intervals^{27–29} or coarse spatiotemporal resolutions^{7,9,30}, leaving key knowledge gaps³¹.

Here we utilize our recent compilation of planktonic foraminifera³², a group of biomineralizing marine plankton, to study the establishment and maintenance of the modern-style LDG at a previously unachieved

spatiotemporal resolution. By examining spatial diversity patterns across 40 million years, we provide fundamental insight on the co-evolution of the biosphere and geosphere and test key hypotheses on LDG drivers^{12,33,34}.

We quantified temporal patterns in LDGs using 434,113 unique species-by-locality-by-time records (Fig. 1a and Supplementary Figs. 1–4). Records older than 40 million years (Myr) were excluded due to poor-quality low-latitude data for earlier time intervals. LDGs were constructed using five subsampling approaches that accounted for sampling biases (Supplementary Methods and Supplementary Fig. 5), all of which reveal substantial changes in the spatial distribution of species over the past 40 Myr (Fig. 1b,c and Supplementary Figs. 6–10). A modern-style LDG began to emerge gradually beginning approximately 34 million years ago (Ma), coincident with the transition from warmhouse to coolhouse conditions, but remained shallow until around approximately 15–10 Ma, contemporaneous with an increase in global cooling³⁵. Gradient (that is, slope) estimates for richness steepened from virtually no gradient at 40 Ma (Fig. 1c) and were insensitive to methodological choice (Supplementary Table 1 and Supplementary Figs. 11–24). This pattern supports previous suggestions that shallower diversity gradients occur during warmer, greenhouse intervals^{7,8,27}.

Modern-day diversity for planktonic foraminifera is richest at mid-latitudes, with a slight depression at the Equator^{16,28}. We fit linear and second-order polynomial models to each of our 16 LDGs to test whether they are better characterized as unimodal or bimodal; data

¹Department of Earth Sciences, University of Oxford, Oxford, UK. ²School of Earth and Environment, University of Leeds, Leeds, UK. ³School of Geographical Sciences, University of Bristol, Bristol, UK. ⁴State Key Laboratory of Tibetan Plateau Earth System, Environment and Resources, Institute of Tibetan Plateau Research, Chinese Academy of Sciences, Beijing, China. ✉e-mail: erin.saupe@earth.ox.ac.uk

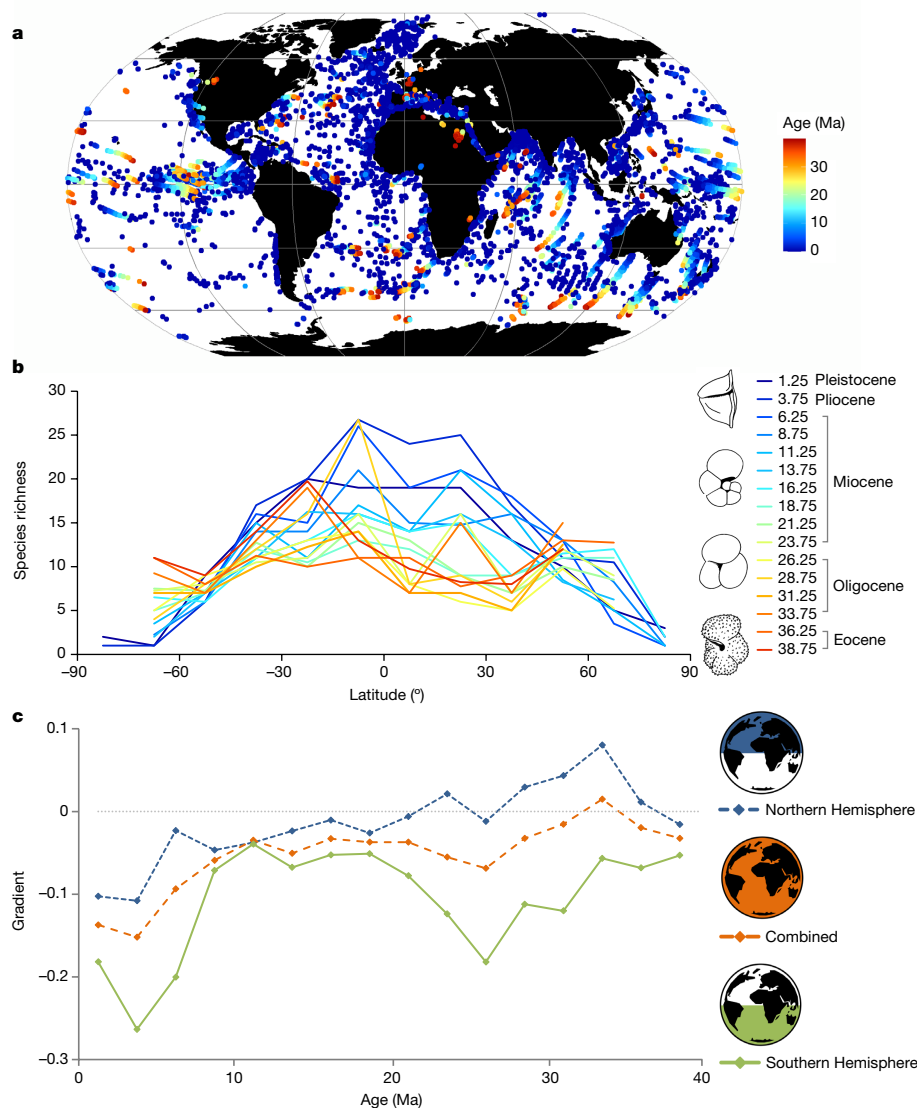


Fig. 1 | The emergence of a modern-day LDG in planktonic foraminifera over the past 40 Myr. a, Data used to quantify LDGs. Points are coloured by the age of the sample. Distributional maps rotated to palaeo-positions for 2.5-Myr intervals are available in Supplementary Fig. 1. The map in **a** was made using the *rgdal* package in R with data from Natural Earth (<https://www.naturalearthdata.com>). **b**, LDGs constructed using unique site-by-age richness estimates in 2.5-Myr time bins (the midpoint age is shown). To generate curves, point-level

data were binned by 15° latitude and richness was estimated using the 75th percentile of the samples in each latitude-by-age bin. Results were robust to the LDG construction method (Supplementary Figs. 6–10) and show that the modern-day LDG emerged only approximately 15 Ma. **c**, Estimates of the gradient (that is, slope) for LDGs over the past 40 Myr using the curves from **b**. Gradients were insensitive to the methodological approach (Supplementary Figs. 11–24) and show a steepening of the gradient towards the present.

for the Northern and Southern Hemispheres were modelled together and individually (see ‘Estimating LDG gradients’). For all time periods other than the most recent (0–2.5 Ma), a linear model produced a better fit (Supplementary Table 2). Peak richness for planktonic foraminifera occurred at higher latitudes from 40 to 20 Ma, but with generally flatter gradients, after which peak richness shifted to approximately 10–20° latitude, consistent with the diversity pattern observed today^{16,28} (Fig. 1b).

To identify potential drivers of LDG changes over the past 40 Myr, we investigated the relationship between richness and environment both spatially within time bins and temporally across time bins. In the first approach, we modelled richness as a function of mean annual sea surface salinity, mean annual mixed-layer depth, mean annual thermocline extent and mean annual sea surface temperature (SST) using spatial autoregressive models within each of the 2.5-Myr time bins (Supplementary Figs. 25–27). After correcting for multiple comparisons, only SST exhibited a consistent and strong positive relationship

with richness over time (Fig. 2). This relationship persisted for at least the past 15 million years, and perhaps longer, but with confidence intervals that overlap zero. Results are insensitive to permutations of the data (Supplementary Figs. 28–32). The temperature range of the thermocline is highly correlated with SST (Supplementary Fig. 26) and therefore could not be included in the multivariate model. When the thermocline temperature range was modelled separately, however, the strength of the relationship was similar to that of SST (Supplementary Fig. 33). No other variables exhibited such a relationship (Supplementary Fig. 33). Richness was not linked to surface ocean area when species richness was modelled as a function of area within 15° latitudinal bins (Supplementary Fig. 34).

In the second model approach, we investigated the relationship between change in richness and change in climate variables at given locations on Earth. Change was examined over 2.5-, 5-, 7.5-, 10- and 12.5-Myr intervals of time (Supplementary Figs. 35 and 36). Change in SST was the only significant predictor of change in richness across

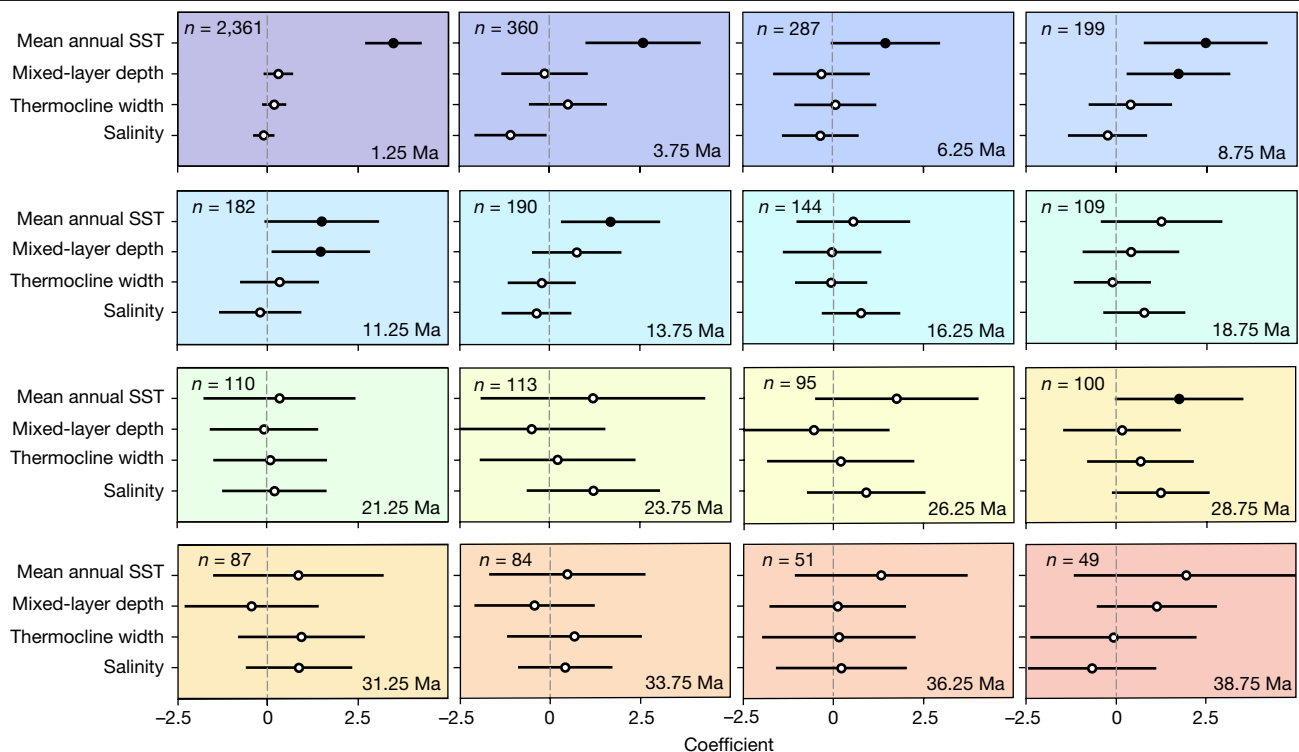


Fig. 2 | Spatial autoregressive model coefficients from analyses examining the relationship between richness and four environmental predictors within 2.5-Myr time bins. The midpoint age for each bin is shown.

Environmental variables include mean annual SST, the log of mean annual mixed-layer depth, the width of the thermocline, and the log of mean annual

salinity. Coefficients are black if significant at an α of 0.05 using the Bejamini and Hochberg correction for multiple comparisons. Results are shown for data that were latitudinally restricted (within 55° latitude) but are consistent with models that include all latitudinal data (Supplementary Fig. 28). Error bars represent 95% confidence intervals around the model coefficient estimates.

these five models, and results were robust to permutations of the data (Supplementary Table 3). No relationship was found when the thermocline temperature range was modelled separately (Supplementary Table 4), but this could reflect the greater uncertainty in estimating temperatures at depth with palaeoclimate models, especially in deep time.

These results and previous work^{16,36,37} suggest species richness for planktonic foraminifera could be explained, at least in part, by steepening of the latitudinal temperature gradient and associated increase in vertical temperature structure at low latitudes^{35,38} over the past 15 Myr, the latter of which may have enhanced niche-partitioning-mediated speciation in the tropics^{39,40}. To further test this hypothesis, we examined the degree to which species of planktonic foraminifera partition by depth within the water column over time and space. We found that low-latitude assemblages of species today are more evenly distributed vertically within the water column across the mixed layer, thermocline and sub-thermocline than are assemblages at high latitudes (Fig. 3). However, assemblages exhibited greater evenness of depth habitats (mixed layer, thermocline and sub-thermocline) across latitudes when the gradient was shallower millions of years ago. This pattern implies that warmer waters at high latitudes supported a broader range of vertical temperature habitats within the water column from 40 to 15 Ma, and that these assemblages collapsed as the high latitudes cooled.

If changes to the vertical structure of the water column facilitated the formation of a modern-style LDG, we would expect higher rates of speciation at low latitudes coincident with the steepening of the diversity gradient, and higher rates of either extirpation and/or extinction at high latitudes. We quantified differential rates of speciation, extinction, extirpation and dispersal in low versus high latitudes, defined as within or exclusive of 30° latitude.

Low-latitude speciation began to exceed high-latitude speciation after 30 Ma, suggesting that the modern-style LDG is possibly driven

by higher rates of low-latitude origination (Fig. 4 and Supplementary Figs. 37–43). These results are consistent with previous findings of higher speciation rates at low latitudes for planktonic foraminifera^{15,41,42}. In addition to low-latitude speciation, local extirpation at high latitudes also contributed to a modern LDG, but tended to have a smaller effect size (Fig. 4 and Supplementary Figs. 37, 38 and 40–43). Previous work²⁹ has found that the redistribution of species' ranges, and not speciation, was important to LDG formation, but this was probably due to the short timescale of their study (that is, the past 3 Myr).

Steepening of the diversity gradient was not driven by extinction, because extinction was higher at low latitudes beginning approximately 20 Ma (Fig. 4 and Supplementary Figs. 37, 38 and 40–43). This heightened extinction dampened the effect of higher speciation in the tropics, but speciation still tended to outpace extinction, adding to richness. Similarly, dispersal from high to low latitudes did not contribute to the emergence of a modern-day LDG, as dispersal dynamics were reversed (that is, occurred predominantly from low to high latitudes) for at least the past 10 Myr (Fig. 4 and Supplementary Figs. 37, 38 and 40–43). Dispersal was usually rapid, with a mean wait time after speciation of 1.7 Myr (± 2 Myr).

The relationship between temperature and richness was dampened for time periods older than 15 Ma. This weakened relationship may reflect climate model inaccuracies that inflate with time, or the fact that richness and temperature do not vary substantially with latitude. In the latter scenario of limited temperature variation, sensitivity analyses suggest that no relationship would be found between richness and temperature (Supplementary Fig. 29). Scarcer data in deep time may also make a relationship with temperature more difficult to obtain (Supplementary Fig. 30), but LDGs constructed with minimal data still return modern-style LDGs towards the present (Supplementary Fig. 31). Excluding sites potentially subject to dissolution only served to strengthen patterns (Supplementary Fig. 32).

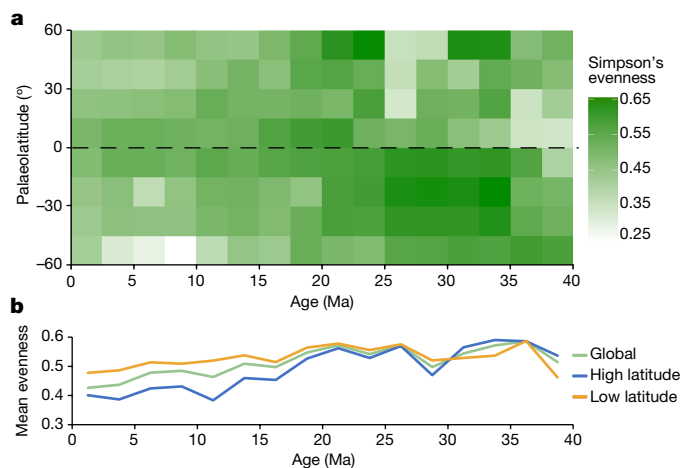


Fig. 3 | The dynamics of depth partitioning for planktonic foraminiferal assemblages across space and time. **a**, We quantified evenness of depth habitat within each unique site-by-age bin using Simpson's index. This metric determines how evenly spread species are among the mixed layer, thermocline and sub-thermocline for a given time and place within the water column. Mean evenness estimates were taken for each 2.5-Myr and 15° latitude bin. Analyses were performed only within 55° latitude, as data were limited at high latitudes earlier in the Cenozoic. **b**, Mean evenness across latitudes for a given 2.5-Myr time bin, for low latitudes (defined as within 30°), high latitudes, and globally. Low-latitude assemblages of species today are more evenly distributed across the mixed layer, thermocline and sub-thermocline than are assemblages at high latitudes. However, assemblages exhibited greater evenness across latitudes when the gradient was shallower millions of years ago. Current knowledge of foraminiferal depth preferences only allowed for measurement of evenness across three depths, but our assumption is that the thermocline and sub-thermocline are subdivided to contain multiple niches, with more niches present at low latitudes during the past 15 Myr, and with more niches present at higher latitudes during warmer intervals compared to today. For the raw evenness data in each sample, see Supplementary Fig. 44.

We were not able to test the relationship of richness with zooplankton biomass⁴³ or nutrient availability⁴⁴ because high-resolution spatial and temporal data for these variables at global scale do not exist for the past 40 Myr. However, the regions with the highest foraminiferal richness, the nutrient-poor subtropical gyres⁴⁵, are characterized by the lowest population densities of planktonic foraminifera⁴⁶. The subtropical gyres have been incredibly stable over tens of millions of years⁴⁷, and may have accumulated their high diversity due to both niche partitioning and reduced extirpation and extinction. It is possible that competition with diatoms or other groups, especially when interacting with seasonal food availability at high latitudes, also structure the LDG for planktonic foraminifera, but seasonality was found to correlate with SST and thermocline temperature range in many time bins and was therefore not included as a predictor in our models (Supplementary Fig. 26).

Together, our results suggest that the modern-day LDG for planktonic foraminifera is controlled, at least in part, by high-latitude cooling that brought colder bottom waters to the tropics, increasing both latitudinal temperature gradients and vertical temperature gradients at low latitudes. The increased vertical temperature structure within the water column at low latitudes may have enhanced niche partitioning, providing more opportunity for speciation over the past 30–15 Myr^{16,36,37}. Cooler high-latitude water may have also served to extirpate regional populations of species. Consistent with our hypothesis, the tropics today are richer than the tropics of the Eocene and Miocene, potentially due to a stronger vertical temperature structure that was weak-to-absent during these warmer time periods. Extreme warmth during the Eocene may have also exceeded the temperature tolerances of species equatorially, further depressing diversity,

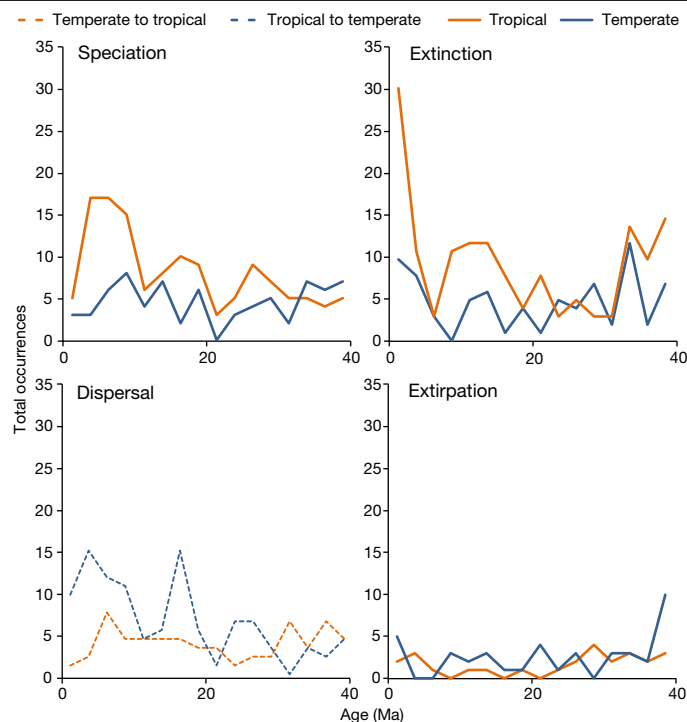


Fig. 4 | Macroevolutionary processes structuring LDGs over the past 40 Myr. The number of speciation (top left), extinction (top right), dispersal (bottom left) and extirpation (bottom right) events in low-latitude (tropical) and high-latitude (temperate) regions. Dispersal quantified the number of species moving from the tropics to temperate regions and vice versa. The steepening of the gradient towards the present-day coincides with enhanced rates of tropical speciation and with higher extirpation from temperate regions. Temperate and tropical regions were defined by 30° latitude for all time periods. Data show results for the approach including all site-by-age records. For proportional patterns, bootstrap subsampling analyses, and results excluding species present in both temperate and tropical regions within a given 2.5-Myr time bin, see Supplementary Figs. 37–43.

an effect that may occur more in the future as the tropics continue to warm^{33,48}. Global diversity for planktonic foraminifera in the Eocene, however, was similar to planktonic foraminiferal diversity today, as species were distributed more evenly across latitudes 40 Ma (Fig. 3).

Our analyses suggest a role for water column structure in facilitating niche partitioning and therefore the emergence of the LDG in planktonic foraminifera. Other potential mechanisms that may have increased low-latitude diversity include the total amount of suitable area vertically within the water column²⁶, metabolic scaling^{42,49} or changes to the biological carbon pump that redistributed nutrients at depth and opened new niches as the climate cooled over the past 15 Myr^{50,51}. This latter mechanism of nutrient redistribution complements the vertical temperature-driven niche separation proposed here.

To conclude, the establishment of the modern-day LDG is consistent with a cooling climate that allowed for elevated speciation via niche partitioning at low latitudes, while restructuring distributions and removing niches at high latitudes. By resolving how spatial patterns of biodiversity have varied through deep time, we provide valuable information on hypothesized causes crucial for understanding how biodiversity is generated and maintained over geological timescales, beyond the scope of modern-day ecological studies.

Online content

Any methods, additional references, Nature Portfolio reporting summaries, source data, extended data, supplementary information,

acknowledgements, peer review information; details of author contributions and competing interests; and statements of data and code availability are available at <https://doi.org/10.1038/s41586-023-05712-6>.

1. Fine, P. V. Ecological and evolutionary drivers of geographic variation in species diversity. *Annu. Rev. Ecol. Evol. Syst.* **46**, 369–392 (2015).
2. Hillebrand, H. On the generality of the latitudinal diversity gradient. *Am. Nat.* **163**, 192–211 (2004).
3. Mittelbach, G. G. et al. Evolution and the latitudinal diversity gradient: speciation, extinction and biogeography. *Ecol. Lett.* **10**, 315–331 (2007).
4. Willig, M. R., Kaufman, D. M. & Stevens, R. D. Latitudinal gradients of biodiversity: pattern, process, scale, and synthesis. *Annu. Rev. Ecol. Evol. Syst.* **34**, 273–309 (2003).
5. Pontarp, M. et al. The latitudinal diversity gradient: novel understanding through mechanistic eco-evolutionary models. *Trends Ecol. Evol.* **34**, 211–223 (2019).
6. Crame, J. A. Taxonomic diversity gradients through geological time. *Divers. Distrib.* **7**, 175–189 (2011).
7. Mannion, P. D., Upchurch, P., Benson, R. B. J. & Goswami, A. The latitudinal biodiversity gradient through deep time. *Trends Ecol. Evol.* **29**, 42–50 (2014).
8. Powell, M. G. Latitudinal diversity gradients for brachiopod genera during late Palaeozoic time: links between climate, biogeography and evolutionary rates. *Glob. Ecol. Biogeogr.* **16**, 519–528 (2007).
9. Powell, M. G., Beresford, V. P. & Colaienne, B. A. The latitudinal position of peak marine diversity in living and fossil biotas. *J. Biogeogr.* **39**, 1687–1694 (2012).
10. Hillebrand, H. Strength, slope and variability of marine latitudinal gradients. *Mar. Ecol. Prog. Ser.* **273**, 251–267 (2004).
11. Beaupre, G., Rombouts, I. & Kirby, R. R. Towards an understanding of the pattern of biodiversity in the oceans. *Glob. Ecol. Biogeogr.* **22**, 440–449 (2013).
12. Tittensor, D. P. et al. Global patterns and predictors of marine biodiversity across taxa. *Nature* **466**, 1098–1101 (2010).
13. Pianka, E. R. Latitudinal gradients in species diversity: a review of concepts. *Am. Nat.* **100**, 33–46 (1966).
14. Saupe, E. E. et al. Spatio-temporal climate change contributes to latitudinal diversity gradients. *Nat. Ecol. Evol.* **3**, 1419–1429 (2019).
15. Stehli, F. G., Douglas, R. G. & Newell, N. D. Generation and maintenance of gradients in taxonomic diversity. *Science* **164**, 947–949 (1969).
16. Rutherford, S., D'Hondt, S. & Prell, W. Environmental controls on the geographic distribution of zooplankton diversity. *Nature* **400**, 749–752 (1999).
17. Klopfer, P. H. Environmental determinants of faunal diversity. *Am. Nat.* **93**, 337–342 (1959).
18. Haffer, J. & Prance, G. T. Climatic forcing of evolution in Amazonia during the Cenozoic: on the refuge theory of biotic differentiation. *Amazoniana* **16**, 579–607 (2001).
19. Dynesius, M. & Jansson, R. Evolutionary consequences of changes in species' geographical distributions driven by Milankovitch climate oscillations. *Proc. Natl Acad. Sci. USA* **97**, 9115–9120 (2000).
20. Dobzhansky, T. Evolution in the tropics. *Am. Sci.* **38**, 209–221 (1950).
21. Williams, C. B. *Patterns in the Balance of Nature* (Academic Press, 1964).
22. Paine, R. T. Food web complexity and species diversity. *Am. Nat.* **100**, 65–75 (1966).
23. Schemske, D. W., Mittelbach, G. G., Cornell, H. V., Sobel, J. M. & Roy, K. Is there a latitudinal gradient in the importance of biotic interactions? *Annu. Rev. Ecol. Evol. Syst.* **40**, 245–269 (2009).
24. Currie, D. J. Energy and large-scale patterns of animal and plant species richness. *Am. Nat.* **137**, 27–49 (1991).
25. Connell, J. H. & Orias, E. The ecological regulation of species diversity. *Am. Nat.* **98**, 399–414 (1964).
26. Rosenzweig, M. L. *Species Diversity in Space and Time* (Cambridge Univ. Press, 1995).
27. Fenton, I. S. et al. The impact of Cenozoic cooling on assemblage diversity in planktonic foraminifera. *Phil. Trans. R. Soc. B* **371**, 20150224 (2016).
28. Yasuhara, M. et al. Past and future decline of tropical pelagic biodiversity. *Proc. Natl Acad. Sci. USA* **117**, 12891–12896 (2020).
29. Yasuhara, M., Hunt, G., Dowsett, H. J., Robinson, M. M. & Stoll, D. K. Latitudinal species diversity gradient of marine zooplankton for the last three million years. *Ecol. Lett.* **15**, 1174–1179 (2012).
30. Jablonski, D., Roy, K. & Valentine, J. W. Out of the tropics: evolutionary dynamics of the latitudinal diversity gradient. *Science* **314**, 102–106 (2006).
31. Yasuhara, M., Tittensor, D. P., Hillebrand, H. & Worm, B. Combining marine macroecology and palaeoecology in understanding biodiversity: microfossils as a model. *Biol. Rev.* **92**, 199–215 (2017).
32. Fenton, I. S. et al. Triton, a new species-level database of Cenozoic planktonic foraminiferal occurrences. *Sci. Data* **8**, 160 (2021).
33. Yasuhara, M. & Deutsch, C. A. Paleobiology provides glimpses of future ocean. *Science* **375**, 25–26 (2022).
34. Yasuhara, M. et al. Time machine biology cross-timescale integration of ecology, evolution, and oceanography. *Oceanography* **33**, 16–28 (2020).
35. Westerhold, T. et al. An astronomically dated record of Earth's climate and its predictability over the last 66 million years. *Science* **369**, 1383–1387 (2020).
36. Al-Sabouni, N., Kucera, M. & Schmidt, D. N. Vertical niche separation control of diversity and size disparity in planktonic foraminifera. *Mar. Micropaleontol.* **63**, 75–90 (2007).
37. Lowery, C. M., Bown, P. R., Fraass, A. J. & Hull, P. M. Ecological response of plankton to environmental change: thresholds for extinction. *Annu. Rev. Earth Planet. Sci.* **48**, 403–429 (2020).
38. Lear, C. H., Elderfield, H. & Wilson, P. A. Cenozoic deep-sea temperatures and global ice volumes from Mg/Ca in benthic foraminiferal calcite. *Science* **287**, 269–272 (2000).
39. Weiner, A., Aurahs, R., Kurasawa, A., Kitazato, H. & Kučera, M. Vertical niche partitioning between cryptic sibling species of a cosmopolitan marine planktonic protist. *Mol. Ecol.* **21**, 4063–4073 (2012).
40. Schneider, E. & Kennett, J. P. Segregation and speciation in the Neogene planktonic foraminiferal clade Globococcone. *Paleobiology* **25**, 383–395 (1999).
41. Raja, N. B. & Kiessling, W. Out of the extratropics: the evolution of the latitudinal diversity gradient of Cenozoic marine plankton. *Proc. Biol. Sci.* **288**, 20210545 (2021).
42. Allen, A. P. & Gillooly, J. F. Assessing latitudinal gradients in speciation rates and biodiversity at the global scale. *Ecol. Lett.* **9**, 947–954 (2006).
43. Irigoien, X., Huisman, J. & Harris, R. P. Global biodiversity patterns of marine phytoplankton and zooplankton. *Nature* **429**, 863–886 (2004).
44. Schiebel, R. & Hemleben, C. *Planktic Foraminifera in the Modern Ocean* (Springer-Verlag, 2017).
45. Ruddimann, W. F. Recent planktonic foraminifera: dominance and diversity in North Atlantic surface sediments. *Science* **164**, 1164–1167 (1969).
46. Bé, A. W. H. & Tolderlund, D. S. in *Micropaleontology of Marine Bottom Sediments* (eds Funnell, B. M. & Riedel, W. K.) 105–149 (Cambridge Univ. Press, 1971).
47. Sibert, E., Norris, R., Cuevas, J. & Graves, L. Eighty-five million years of Pacific Ocean gyre ecosystem structure: long-term stability marked by punctuated change. *Proc. Biol. Sci.* **283**, 20160189 (2016).
48. Chaudhary, C., Richardson, A. J., Schoeman, D. S. & Costello, M. J. Global warming is causing a more pronounced dip in marine species richness around the equator. *Proc. Natl Acad. Sci. USA* **118**, e2015094118 (2021).
49. Worm, B. & Tittensor, D. P. *A Theory of Global Biodiversity* (Princeton Univ. Press, 2018).
50. Boscolo-Galazzo, F. et al. Temperature controls carbon cycling and biological evolution in the ocean twilight zone. *Science* **371**, 1148–1152 (2021).
51. Boscolo-Galazzo, F. et al. Late Neogene evolution of modern deep-dwelling plankton. *Biogeosciences* **19**, 743–762 (2022).

Publisher's note Springer Nature remains neutral with regard to jurisdictional claims in published maps and institutional affiliations.

Springer Nature or its licensor (e.g. a society or other partner) holds exclusive rights to this article under a publishing agreement with the author(s) or other rightsholder(s); author self-archiving of the accepted manuscript version of this article is solely governed by the terms of such publishing agreement and applicable law.

© The Author(s), under exclusive licence to Springer Nature Limited 2023

Methods

Choice of taxon

Planktonic foraminifera are a group of unicellular, biomineralizing marine plankton that originated approximately 170 Ma in the Early to Middle Jurassic⁴⁴. They are an important component of the plankton from the high latitudes to the Equator in all ocean basins. Species of planktonic foraminifera occupy a range of ecological niches in the upper two kilometres of the open ocean: some live in the surface mixed layer and host algal photosymbionts, whereas others live within or below the thermocline and feed primarily on sinking phytodetritus⁴⁴.

Owing to their global abundance and preservation potential, planktonic foraminifera have been demonstrated to have the best species-level fossil record of the past 66 million years⁵². The quality of this fossil record permits an exceptionally high-resolution view into past species distributions, ecologies, and life histories. Recent work compiling this information into the single, harmonized Triton database³² allows us to investigate the drivers and patterns of LDGs at greater fidelity than possible before.

Description and preparation of the data

We quantified temporal patterns in LDGs using 434,113 unique species-by-locality-by-age records from the Triton database³², which represents the single largest dataset for any fossil group. Data were curated for taxonomic consistency, and all ages were converted to the Geological Time Scale (GTS) 2020 timescale. Following previous work³², occurrences substantially outside the known age range of a species were excluded, using a threshold of 2 Myr for the Neogene and 5 Myr for the Palaeogene; such records are likely to be taxonomic misidentifications or the result of reworking. Spatial coordinates were rotated to their past position (palaeo-coordinates) based on a previous study⁵³. Spatial imprecision in coordinates may occur due to error in the palaeo-coordinate rotation plate model, and/or from ocean currents displacing foraminiferal tests as the dead organisms sank to the seafloor. However, neither source of error is likely to have large effects on the LDG patterns quantified here, given the spatial resolution of our analyses (usually 15° latitude bins, or roughly 1,500 km; see the section ‘Spatiotemporal bin selection’). For example, for sites less than 1 km depth or for large foraminifera, the distance between where the organism died and where it settled is unlikely to be larger than approximately 100 km (refs. ^{54,55}). For depths of 2–3.5 km, a maximum displacement of 100–400 km is reasonable^{56,57}. We limited analyses to the past 40 Myr because poor-quality data at low latitudes early in the Cenozoic made it challenging to accurately calculate richness for these early intervals.

Quantifying temporal patterns for LDGs over 40 Myr

We estimated LDGs using percentiles from point-occurrence data and by calculating central tendencies using three different subsampling methods, described below. All analyses used the R v.4.1.3 computing environment⁵⁸.

Spatiotemporal bin selection. LDGs were constructed by calculating richness within spatiotemporal bins. Numerous binning schemes were tested to evaluate the sensitivity of patterns to spatiotemporal resolution. Eight temporal bin durations were tested, from 2.5 Myr to 20 Myr, in 2.5-Myr increments. Temporal binning may inflate species counts⁵⁹, and thus bin duration should be narrower than the average duration of species⁶⁰. For the planktonic foraminiferal species studied here, median species’ duration was 5.96 Myr, suggesting that bin durations longer than this will suffer from greater time averaging. We therefore focused analyses on the shortest temporal duration (2.5 Myr) but present results for other schemes (Supplementary Figs. 7–9 and 14). Longer temporal bins give steeper gradient estimates, but overall patterns remain consistent, as can be seen when rescaling richness in

each time bin (Supplementary Fig. 14). The spatial distributions of data at a resolution of 2.5 Myr are shown in Supplementary Fig. 1.

We tested eight latitudinal bin resolutions, from 2.5° to 20°, in steps of 2.5°. We aimed to use the highest spatial bin resolution, while ensuring sufficient data to calculate LDGs within 2.5-Myr time bins. Therefore, to choose an ‘optimum’, we eliminated binning schemes that resulted in an empty set (no data) for latitudinal bins in any 2.5-Myr time bin. We further eliminated any binning scheme with insufficient data (defined here as 15 samples, five sites and 150 records) in at least five latitudinal bins for any time bin. This approach identified 15° latitude bins as the highest ‘ideal’ resolution for analyses.

Analyses focused on a spatiotemporal resolution of 2.5 Myr and 15° latitude (Supplementary Figs. 2–4), which was sufficiently sensitive to return the known, modern-day LDG with a slight equatorial dip^{16,28} (Fig. 1b). Estimates of the LDG using other spatial binning schemes produced similar results (Supplementary Figs. 7–9), and latitudinal resolution did not have a strong influence on gradient estimates (Supplementary Fig. 15).

Point-occurrence method for LDGs. LDGs were quantified using unique site-by-age richness estimates within each 2.5-Myr time bin. Analyses excluded samples in which the aim of the study was to identify selected species only, or in which preservation was marked as poor (less than 10% of the data).

To generate LDG curves, point-level data were binned by 15° latitude. Richness was estimated using the 75th percentile of the samples in each latitude-by-age bin. Changes in the LDG through time were not affected by choice of percentile (Supplementary Figs. 6 and 12). Percentiles were used to estimate LDGs because planktonic foraminiferal assemblages are more likely to be characterized by low richness due to dissolution or incomplete community counts, rather than high richness from time averaging, particularly given the short temporal bins used here. Furthermore, modern diversity patterns are characterized by the most diverse sites in a given latitude; for example, in many clades, the tropics today house both very low and very high species richness dependent on the location and environment⁶¹.

Subsampling method for LDGs. To test whether point-level LDG patterns remained consistent when accounting for variation in data quantity, we estimated LDGs using three subsampling approaches. For each latitude-by-age combination, 1,000 subsamples were drawn at random with replacement and the number of unique species was counted. The mean of the 1,000 subsamples served as the richness estimate for that latitude-by-age bin, with associated 95% confidence intervals.

Three different subsampling methods were used: (1) by site, (2) by sample, and (3) by record (Supplementary Fig. 5). The ‘by site’ method divided the dataset on the basis of locality (or site) and selected a set number of sites for a given latitude-by-age bin. Richness was calculated from all species at the selected sites within that bin, irrespective of their exact age. We varied the number of sites selected from 3 to 20 ($n = 3, 5, 10, 15$ and 20). We focused on five sites because it allowed for the maximum number of spatiotemporal bins and produced narrower confidence intervals than when subsampling using three sites, but results were broadly insensitive to site number (Supplementary Figs. 9 and 18).

The ‘by sample’ method of subsampling divided the dataset on the basis of both locality and age and selected a set number of unique site-by-age samples from a given latitude-by-age bin. Each sample therefore represents the foraminiferal assemblage alive at a given time. The richness was calculated from unique species in the selected assemblages. We varied the number of samples selected from 10 to 50 in increments of 5. We selected 15 samples on the basis of the trade-off between the maximum number of samples and the narrowest confidence intervals (Supplementary Figs. 7 and 19).

The ‘by record’ method of subsampling divided the dataset on the basis of locality, age and species, and selected a set number of unique species records from any site or age within a given latitude-by-age bin.

Each record represented one row in the Triton dataset. The richness was calculated as the number of unique species within the selected records. We selected from 100 to 500 records in intervals of 50. We focused on 150 records, but results were broadly insensitive to record number (Supplementary Figs. 8 and 20).

In contrast to point-level LDG construction, we did not exclude data in which the aim of the study was to identify selected species, and in which preservation was marked as poor, because subsampling does not assume any one sample is representative. Comparisons of point-level and subsampled LDG estimates show similar patterns (Supplementary Figs. 10, 23 and 24), although subsampling tended to suggest higher average species richness. Higher richness in subsampled LDGs may reflect the influence of spatiotemporal averaging, which can inflate richness estimates. Alternatively or additionally, incomplete sampling or dissolution might lower richness in the point-level estimates.

Estimating LDG gradients. The strength (or gradient) of LDGs was estimated using a linear model of richness as a function of latitude. For point-level data, richness estimates from the same site and time bin were characterized by the 50th, 60th, 75th and 90th percentiles to avoid pseudo-replication. We focused on patterns using the 75th percentile, but results were insensitive to percentile choice (Supplementary Figs. 6, 12 and 13). To ensure that gradient estimates were comparable over time, we calculated gradients only within 55° latitude, as older time periods were characterized by sparse high-latitude data. However, results were insensitive to latitudinal extent (Supplementary Fig. 11).

Gradients were estimated individually for the Northern and Southern Hemispheres, and for both hemispheres combined using absolute latitude. We tested whether a model with separate slopes for each hemisphere provided a significantly better fit to data than a combined model using Akaike information criterion adjusted for small sample sizes (AICc). For most time periods ($n = 11$ of 16), a model that used data from both hemispheres was preferred over a model with separate gradients (Supplementary Table 1). Combining the two hemispheres increased the data on which a gradient was calculated.

We calculated gradients on rescaled richness to investigate the influence of variation in richness through time on gradient estimates (Supplementary Figs. 11–13). Richness was rescaled by setting maximum richness within a time bin to one. Rescaling affected the steepness of the latitudinal gradient but allowed for more direct comparisons of LDG shape across time. LDGs with peak richness in equatorial regions will have a steeper rescaled gradient than gradients in which peak richness is in the mid-latitudes.

We compared gradients estimated from point-level LDGs to gradients estimated from subsampled LDGs. Gradients were calculated for each subsampling iteration and every latitude-by-age bin combination (Supplementary Fig. 16), from which we derived mean and 95% confidence intervals (Supplementary Figs. 14, 15 and 18–21). Using the median instead of the mean produced almost identical results (Supplementary Fig. 17). Latitude-by-time bin resolution influenced gradient estimates but did not mask overall patterns (Supplementary Figs. 14 and 15). Choice of age bin exaggerated latitudinal differences because broader age bins tended to result in more time averaging, but overall patterns were similar (Supplementary Fig. 14). Similarly, choice of subsampling method had little effect, although the use of sites tended to produce broader confidence intervals (Supplementary Figs. 21, 23 and 24). The amount of subsampling affected the steepness of the gradient, but not the overall shape, and rescaling removed this effect (Supplementary Figs. 18–20). Visual inspection of gradients suggested that the slopes of the Northern and Southern Hemispheres, for all time periods, were mirrored (Supplementary Fig. 16).

Finally, we calculated and compared gradients from raw richness tallied directly from species counts in each latitude-by-age bin (Supplementary Fig. 22), finding similar overall patterns to the subsampled and point-level gradients.

Estimating bimodality. Shallow gradients may indicate minimal differences in richness across latitudes or may indicate that bimodality was more pronounced during these times. To distinguish between these two possibilities, we compared a linear model with a second-order polynomial model using AICc (Supplementary Table 2).

Identifying LDG drivers over the past 40 Myr

Diversity dataset. We investigated possible LDG drivers over the past 40 Myr by coupling atmosphere–ocean generalized circulation models (AOGCMs) to point-level richness estimates within 2.5-Myr time bins. To avoid pseudo-replication, a single, mean richness estimate was calculated for each climatic grid cell.

Palaeoclimate simulations. To explore whether palaeoclimate influenced the biogeographical distribution of planktonic foraminifera, we utilized a newly updated version of a state-of-the-art palaeo-general circulation model.

Palaeoclimate model. Palaeoclimate model simulations were carried out using a recent version of the UK Met Office coupled AOGCM, referred to as HadCM3 or HadCM3L-M2.1D following the nomenclature of ref. ⁶². HadCM3L-M2.1D has a model resolution of 3.75° longitude × 2.5° latitude in the atmosphere and ocean (approximately 250-km grid squares in the tropics), with 19 hybrid levels in the atmosphere and 20 vertical levels in the ocean. Equations were solved on the Arakawa B-grid. As is common in all climate models, subgrid-scale processes, such as cloud, convection and oceanic eddies, were parameterized because they cannot be resolved at the scales required (usually metres to several kilometres) for model resolution.

Owing to scarce spatiotemporal data recording land-surface vegetation and soil characteristics in deep time, we used modern-day vegetation expressions for broadleaf trees, deciduous trees, shrubs, C3 and C4 grasses (five in total), and a globally uniform distribution of medium loam soil characteristics in the model land-surface scheme (MOSES 2.1)⁶³. The land-surface scheme also included evaporation from subgrid-scale lakes, which were prescribed as a lake fraction in each grid box at the start of the simulation. We used a version of the model that included the dynamical vegetation model TRIFFID (top-down representation of interactive foliage and flora including dynamics). TRIFFID predicts the distribution and properties of global vegetation based on plant functional types in the form of fractional coverage (and thus plant functional type coexistence) within a grid-cell, based on competition equations using the climate tolerance of five plant functional types.

The model included a further update that modified cloud condensation nuclei density and cloud droplet effective radius, following recent work^{64,65}. This modification raised temperatures at high latitudes, without substantially changing tropical temperatures, which reduced the pole-to-Equator temperature gradient in line with proxy observations. This update was found to work under hot, cool and icehouse conditions, as well as under pre-industrial boundary conditions, making it appropriate for use across modern and deep time.

The ocean model was based on the model of Cox et al.⁶⁶ and is a full primitive equation with a three-dimensional model of the ocean. A second-order numerical scheme was used along with centred advection to remove nonlinear instabilities. Flux adjustments—such as artificial heat and salinity adjustments in the ocean component model⁶⁷ to prevent them from drifting to unrealistic values—were not required in this model, which is a crucial feature for long palaeoclimate simulations⁶⁸. Sea ice was calculated on a zero-layer model; partial sea-ice coverage was possible, with a consistent salinity assumed for ice.

Each simulation was initialized from an equilibrated pre-industrial state in the atmosphere and ocean. Surface vegetation was uniformly set as shrub everywhere and allowed to evolve via TRIFFID based on the evolution of the local climate.

The HadCM3 family of models has contributed extensively to the Coupled Model Intercomparison Project (CMIP 1–5) experiments and the Paleoclimate Modelling Intercomparison Project (PMIP 1–4), and has demonstrated skill at reproducing the modern-day climate⁶² and palaeoclimate in an array of experiments^{69–71}. Palaeoclimate experiments require hundreds of years to reach a near-surface equilibrium state but substantially longer (many thousands of years) for the deep ocean^{68,69}; even longer is required for true climate equilibrium, owing to the long period of adjustment of ocean circulation to applied forcings. Lower-resolution models are less computationally expensive, allowing fully equilibrated simulations of deep time climate, which would not be possible with higher-resolution, more complex models.

Snapshot simulations, specific boundary conditions and spin-up. We ran nine ‘snapshot’ simulations over the past 40 Myr of the Cenozoic, with each simulation having time-specific boundary conditions. Palaeogeographical digital elevation models (DEMs) were produced by the EarthByte group as part of the PALEOMAP project⁷². Each stage and time-specific DEM were interpolated from a $1^\circ \times 1^\circ$ grid onto the HadCM3L $3.75^\circ \times 2.5^\circ$ grid. Similarly, land ice was transformed onto the model grid assuming a simple parabolic shape to estimate the height (m) of ice sheets. ‘Realistic’ $p\text{CO}_2$ concentrations for each simulation were based on previous work⁷³. Time-specific solar luminosity for each simulation was based on ref. ⁷⁴. All other boundary conditions, such as orbital parameters, volcanic aerosol concentrations, and so on, were held constant at pre-industrial values.

To ensure each simulation had fully adjusted to the boundary conditions, we followed a three-stage spin-up protocol so that each simulation was fully equilibrated: (1) the globally and volume-integrated annual mean ocean temperature trend was less than 1°C per 1,000 years; (2) trends in surface air temperature were less than 0.3°C per 1,000 years; and (3) the net energy balance at the top of the atmosphere, averaged over a 100-year period at the end of the simulation, was less than 0.25 W m^{-2} . In general, these simulations were run for over 9,000 model years to ensure full Earth system equilibrium. Climate means were produced from the past 100 years of each simulation.

Spatiotemporal interpolation techniques. Using the climatic snapshot climate simulations, we interpolated model data and boundary conditions over the past 40 Myr. First, the DEM (bathymetry and topography) was interpolated linearly between each pair of snapshot simulations at 0.5-Myr increments onto a $1^\circ \times 1^\circ$ longitude by latitude grid. Each increment was time weighted between the two snapshot simulations using the DEMs. The land–sea mask was generated for each newly generated DEM, in which any grid box above 0 m was taken as land and any grid box below 0 m as ocean. Isolated ocean points were removed if six of the surrounding grid boxes were land, with the corresponding topography set as the mean of the surrounding grid boxes.

The snapshot model data (for example, SST and sea surface salinity) were interpolated using bicubic remapping for each variable onto the interpolated land–sea mask. Environmental parameter fields (for example, SST and salinity) were extrapolated to fill in grid boxes that were newly created using Poisson’s equation (elliptic partial differential equation) over the input domain.

Palaeoclimate model uncertainties. Global-scale biodiversity data require global-scale environmental datasets, such as SST. Global proxy databases with large spatiotemporal coverage are available for past time periods, but proxy evidence is limited deeper in time and is increasingly less well-constrained, necessitating the use of palaeoclimate models to provide these global datasets. However, simulating palaeoclimate is challenging. This challenge stems, in part, from the many parameters that may be unconstrained for deeper time observations. Uncertainties can be partitioned into two main sources: (1) boundary condition uncertainty, and (2) model uncertainty.

(1) Boundary conditions are spatiotemporally varying parameters that are required by climate models, but which cannot be calculated internally by the model and instead need to be provided by the user. The most important boundary conditions for the model used here are: (i) palaeogeographical reconstructions, (ii) ice sheet height and extent, (iii) solar luminosity, (iv) orbital configuration, and (v) greenhouse gas concentrations.

(i) A large source of uncertainty arises from palaeogeographical reconstruction. DEMs, constrained by palaeo-databases, provide topography, bathymetry and land–sea concentration. These DEMs are crucial for determining local, regional and global atmospheric and ocean circulation, and therefore the climate in the model. The deeper in time, the less proxy data are available, which results in greater uncertainty in these reconstructions. However, our understanding of plate tectonics, spreading ridges, weathering rates and basinal deposition allows for accurate first-order approximation of deep-time palaeogeography, especially over the past 40 Myr. The largest uncertainties usually result from the height and depth of topographical and bathymetric surfaces and their spatial coverage because of proxy uncertainty (for example, see ref. ⁷⁵).

(ii) Ice sheets (and associated sea-level height) can have a large effect on regional climate and global climate, primarily due to changes in land surface area, planetary albedo and modification to ocean and atmospheric circulation. Currently, most palaeoclimate models prescribe the height and extent of ice sheets based on proxy evidence.

(iii) Solar luminosity, which is the amount of energy received by a planetary body from its parent star, is fairly well known. Gough⁷⁴ approximated the amount of energy based on a simple model using the age of the parent star. Apart from the first 0.2 billion years of Earth history, this approximation is shown to agree well with observations⁷⁶.

(iv) Orbital configuration (the eccentricity, obliquity and precession of the orbit of the planet around its parent star and rotation on its own axis) can have a substantial effect on the seasonal and latitudinal climate signal, which, in turn, can lead to major changes in climate state (glacial to interglacial cycles). These effects are due to ice-sheet formation and associated changes in global atmospheric and oceanic response. For deep-time simulations, a modern orbital configuration is often imposed. There are several reasons for this. First, chronological uncertainty in proxies that are used in model comparison will cover many orbital cycles, which may result in the proxy being more representative of a mean orbital state (akin to the modern day). Second, using a modern configuration makes it easier to understand how different a deep-time climate is than the modern climate. Orbital variation will have its largest effect on climate where ice sheets can grow, which is partly reflective of the amount of $p\text{CO}_2$ in the atmosphere and associated global temperature.

(v) Greenhouse gas concentrations, and more specifically $p\text{CO}_2$ concentrations, are variable through the geological past. Proxy type, age, techniques and calibration uncertainty when converting to a $p\text{CO}_2$ estimate, as well as the number of records through the geological past, can make constraining a deep-time $p\text{CO}_2$ concentration problematic⁷³. Furthermore, although a combination of multiple proxy sources can improve the robustness of the estimated $p\text{CO}_2$ estimates, it may prove problematic in situations where the errors are combined to produce a mean $p\text{CO}_2$ estimate. Time averaging is also an issue. Although palaeogeography changes on geological timescales, $p\text{CO}_2$ concentrations can vary on hundreds to million-year timescales. Here we were only interested in the long-term background signal (millions of years), with scatter around the mean, typically approximately 400 ppm⁷³.

(2) Although all globally available palaeoclimate models use the same well-known equations to simulate the large-scale behaviour of

the atmosphere and ocean, results from different models can vary, in particular, at the local and regional scale. This variation is due to the complexity of each model, resolution dependencies, spin-up and applied initial state, and parameterizations used to approximate processes such as cloud formation that cannot be explicitly resolved at the grid scale of all current palaeoclimate models. In an ideal world, such palaeoclimate simulations would be run by multiple palaeoclimate modelling groups, as is done in the CMIP for near-future climate change studies. Unfortunately, such palaeoclimate comparisons are not currently possible; for instance, these simulations took over two years to complete on a high-performance supercomputer, and few palaeoclimate modelling groups have the capability to set up such deep-time simulations. However, confidence in the robustness of our results can be obtained by the fact that: (1) the HadCM3 family of models, although 20 years older than many contemporaries, still compares reasonably well with models from the previous IPCC coupled CMIP fifth assessment models⁶². (2) HadCM3L-M2.1D has seen continued development⁶². Here we used an updated version of the model that solves a persistent problem in the majority of palaeoclimate models known as the 'cold pole paradox', in which simulated higher latitude temperatures were previously much cooler than suggested by proxy observations. (3) These simulations have been run for over 9,000 model years. Palaeoclimate simulations are usually run for only a couple of thousands of years due to computational costs. However, it can take upwards of 5,000 years to allow a model simulation to equilibrate to all the applied model forcings, especially for the deep ocean, and, as such, for global ocean circulation to be fully representative of the deep-time period. (4) Although model uncertainty is important to constrain, it has been shown that scenario uncertainty (that is, the applied boundary conditions) is a larger source of error, at least for future climate simulations⁷⁷.

Climate and environmental drivers. Environmental constraints on planktonic foraminifera. We investigated nine environmental variables previously posited to constrain the distributions of planktonic foraminifera⁴⁴, including mean annual SST, seasonal variation in SST, mean annual mixed-layer depth, seasonality of the mixed-layer depth, mean annual sea surface salinity, seasonality of sea surface salinity, the width of the thermocline, the temperature range within the mixed layer, and the temperature range within the thermocline (Supplementary Figs. 25–27).

Surface temperature estimates were calculated at a water depth of 5 m. Temperatures within the water column were highly correlated with surface temperatures and therefore were not included in model comparisons. Temperature seasonality was estimated as the standard deviation of monthly variations. HadCM3 estimates potential temperatures (that is, removing the effect of pressure). Planktonic foraminifera are more likely to respond to actual temperature, but the difference between potential and actual temperature is small (less than 1 °C at 1,000 m) and thus we did not correct for this effect.

Surface salinity was calculated at a water depth of 5 m. Salinity deeper in the water column was highly correlated with surface salinity and therefore not included in model comparisons. Seasonality in salinity was estimated as the standard deviation of the monthly variations. Extremes of salinity, whether high or low, may exceed planktonic foraminiferal species' tolerances, whose salinity optimum sits around 35 practical salinity units (PSU)⁴⁴. Therefore, the expected relationship with salinity is thought to be polynomial on the original scale. However, we have insufficient data to model polynomials for many of the time intervals, and thus to model the effect of salinity, we calculated the absolute difference from this optimal salinity value. By using an absolute difference from the optimum, we converted the relationship to approximately linear, with high richness close to the optimum and low richness at the extremes.

For water column structure, we estimated annual mean width of the mixed layer, seasonal variation in the mixed-layer depth and annual mean width of the thermocline. The mixed layer refers to the top of the water column, where environmental conditions are relatively homogeneous and stable due to mixing. Mixed-layer depth was derived from HadCM3L output, which used a Kraus–Turner⁷⁸ bulk mixed-layer approach that calculated a balance between the energy available for mixing the water column and the introduction of buoyancy at the ocean surface. For more detail, see ref. ⁷⁹.

The thermocline is the section of the water column below the mixed layer where temperature changes rapidly with depth. Below the thermocline, temperature is relatively stable. On a rescaled temperature profile (in which the temperature and depth axes are rescaled from 0 to 1), the base of the thermocline was calculated as the point where the gradient steepens past a –1:1 line using a loess function in the base R stats package⁸⁸. We chose a span $\alpha = 0.4$ based on sensitivity analyses: if the span is too large, the regression will be over-smoothed, whereas if the span is too small, large variance will result.

For water column temperature structure, we calculated the mean temperature range within the mixed layer and thermocline based on their identified boundaries, as described above. The temperature range within the thermocline and mixed layer provided a proxy for the diversity of temperature niches at depth within the water column.

Maps for the environmental variables can be found in Supplementary Fig. 25.

Variable selection. The interpolated AOGCM data provided mean global estimates for each of the nine variables at 2.5-Myr intervals. Shallow-water grid cells (water depth of less than 200 m) were excluded for each time bin, based on a Scotese bathymetry model⁷². Removing shallow-water cells excluded coastal environments where planktonic foraminifera communities may be limited by environmental conditions⁴⁴. Mixed-layer depth (mean and seasonality) and salinity (mean and seasonality) were log-transformed to correct for nonlinearity. Variables were centred and rescaled within each 2.5-Myr time bin to better interpret the intercept terms and to ensure similar units for regression coefficients.

The environmental variables were highly collinear with each other in most time periods (Supplementary Fig. 26). We tested for multicollinearity within each of the 2.5-Myr time bins using variance inflation factors (VIFs). Analyses relied on the 'vif' function in the HH R package v.3.1.47 (ref. ⁸⁰). To include the same set of environmental predictors across the 16 time bin models, we limited analyses to those variables with VIFs < 2 in each time interval, following ref. ⁸¹. The final variable set included mean SST, mean annual mixed-layer depth, mean annual sea surface salinity and width of the thermocline. The mean thermocline temperature range was also considered of interest, but was too strongly correlated with mean SST to be included in the same models (that is, the mean R^2 for a model between these two variables was 0.886 across time bins).

We assessed the relationship of these four variables with richness using both multivariate and univariate models (Supplementary Figs. 28–33). For univariate analyses, we included thermocline temperature range alongside the other four predictors (Supplementary Fig. 33).

Model building and calibration. Identifying LDG drivers within time intervals. We modelled the relationship between richness and the four selected environmental predictors within each 2.5-Myr time bin using spatial autoregressive models. Models were fit using the errorsarlm function in the spatialreg R package v.1.2.3 (ref. ⁸²). We adjusted significance levels ($\alpha = 0.05$) to account for multiple comparisons by applying the Benjamini and Hochberg correction⁸³. The optimum neighbourhood distance was calculated for each time period, between 500 km and the distance where autocorrelation becomes nonsignificant, following

ref.⁸⁴, using AIC. Models were checked for heteroscedasticity. We restricted analyses to within 55° latitude, because older time periods lacked data at high latitudes. Using all latitudinal data, rather than limiting analysis to within 55° latitude, produced similar results (Supplementary Fig. 28).

Model exploration and sensitivity analyses. We explored the effects of sampling and preservation on within-age-bin model results. Sampling in the fossil record varies over time, with older time bins typically characterized by fewer data points. Data loss can potentially mask relationships between the predictors and species richness (Fig. 2). We therefore explored whether the results held when fewer data points were used for within-age-bin models. Specifically, in each time bin, data were subsampled to include the same number of data points as the most data-poor time bin ($n = 49$, for 37.5–40 Ma), iterated 100 times. To summarize these results, we used the mean coefficient and standard error from the 100 subsampling iterations for each time bin. Model results removed any statistically significant relationship between temperature and richness, even for more recent time periods, but coefficients were similar (Supplementary Fig. 30). Modern-day LDGs constructed from the more limited data show similar patterns to those constructed on the full dataset (Supplementary Fig. 31).

Dissolution increases with water depth as the carbonate ion concentration and calcite saturation state decrease. Dissolution can artificially reduce richness at a particular site and time as a function of ocean basin depth and the species present, because certain species are more susceptible to dissolution⁴⁴. The differential impact of dissolution may obscure the relationship between environmental variables and species richness. We assessed the potential effect of dissolution on model results by excluding samples with species richness in the lowest 25th percentile, based on 15° latitude and 2.5-Myr age bins. Model results suggested similar relationships and patterns (Supplementary Fig. 32).

The warmer, greenhouse conditions on Earth approximately 40 Ma limited temperature variability across latitudes. Reduced temperature variation may obscure any relationship of temperature with species richness. We therefore tested whether a relationship between temperature and richness can be detected in more recent time bins, when analyses were limited to the range of temperatures characteristic of warmer times. We identified the time bin with the smallest temperature range (35–37.5-Ma time bin, with a temperature range from 15.25 °C to 33.38 °C) and restricted analyses for the other time bins to this temperature range. Using this approach resulted in some time bins having an even narrower temperature range, as time bins towards the present do not have temperatures reaching 33 °C.

When a narrow temperature range was used, the relationship between temperature and richness was lost for most time bins, aside from the most recent (Supplementary Fig. 29). Limiting analyses to a narrower temperature range suggested that no relationship exists between temperature and species richness, even for more recent time bins. Thus, the absence of a relationship between richness and temperature for deeper time bins may reflect this narrower temperature range, which itself may have increased species richness across latitudes.

Identifying LDG drivers through time. In addition to investigating the relationship between potential environmental drivers and richness within time bins spatially, we examined the degree to which change in environmental variables drives change in richness at given sites. To compare shorter-term and longer-term trends, differences were calculated using a range of temporal gaps (from 2.5 Myr to 12.5 Myr, in 2.5-Myr steps). For each temporal gap, we modelled the change in species richness as a linear function of the change in the selected environmental variables. Only a subset of the data used for spatial, within-time analyses could be used for the across-time analyses: to be included, sites were required to have pairs of samples with the requisite

time gap (Supplementary Figs. 35 and 36). Analyses with longer time gaps had fewer data points (Supplementary Table 3).

We ran both multivariate and univariate models; for the latter, we included analysis of the thermocline temperature range (Supplementary Table 4). Richness was estimated as the mean richness for each site within each 2.5-Myr time bin. Analyses used values for the environmental variables on their original scale, rather than rescaled values. Because separate models were run for different time gaps, we adjusted significance values ($\alpha = 0.05$) following the Benjamini and Hochberg correction⁸³. Results were insensitive to latitudinal extent (Supplementary Tables 3 and 4).

The effect of ocean area on species richness. Open ocean area has been hypothesized to drive the LDG, because area is found to correlate positively with species richness today²⁶. To test whether this relationship holds through time for planktonic foraminifera, we modelled richness as a function of open ocean area within 15° latitude and 2.5-Myr time bins (Supplementary Fig. 34). Open ocean area was defined as the area of grid cells with depths of more than 200 m based on the Scotese bathymetry models⁷². We quantified area using the areaPolygon function in the geosphere R package⁸⁵.

Depth partitioning across space and time

Species of planktonic foraminifera live at different depths in the water column, down to about 2 km⁴⁴. Depth preferences for fossil species can be estimated using the isotopic signature of their shells and are usually divided into mixed-layer, thermocline and sub-thermocline dwellers⁵². We investigated how the depth structure of planktonic foraminiferal assemblages changed across space and time. For each unique site and time bin, we partitioned species by three depth categories (mixed-layer, thermocline and sub-thermocline dwellers). We classified the single species inferred to occur across multiple depths (*Chiloguembelina ototara*) as a mixed-layer dweller, as it possessed photosymbionts.

We quantified evenness of depth habitat within each unique site-by-age with Simpson's index using the diversity function in the vegan R package v.2.5-7 (ref.⁸⁶). This metric determined how evenly spread species are among the three depths for a given time and place. That is, highly even assemblages would have roughly equal numbers of species in each depth class, whereas uneven assemblages would vary more in species count by depth class. We excluded sites most likely to be subject to dissolution, defined as those that fell in the lowest 25th percentile of species richness for a given site and time. The mean of these evenness estimates was taken for each 2.5-Myr and 15° latitude bin (Supplementary Fig. 44). Analyses were performed only within 55° latitude, given the sparse data at high latitudes earlier in the Cenozoic (Fig. 3).

Current knowledge of foraminiferal depth preferences only allowed for measurement of evenness across three depths over the past 40 million years. Our assumption, however, is that the thermocline and sub-thermocline are subdivided to contain multiple thermal niches, with more niches available during warmer conditions earlier in the Cenozoic across latitudes, and more niches available at low latitudes during the past 15–10 Myr. The mixed layer is unlikely to be as subdivided, given that conditions within are more homogenous.

Speciation, extinction and dispersal dynamics

To determine the macroevolutionary processes structuring LDGs, we quantified spatial patterns of speciation, extinction, extirpation and dispersal in planktonic foraminifera over the past 40 Myr. Specifically, we investigated whether species originated and went extinct in tropical or temperate regions, whether they dispersed primarily into or out of these regions, and whether they were extirpated (went regionally extinct) at higher rates in one region over the other (Fig. 4 and Supplementary Figs. 37–43). As our focus is on latitudinal patterns, not climatic patterns, we defined the separation between tropical and

temperate regions as 30° for all time periods. We selected 30° because modern-day richness for planktonic foraminifera peaks in the subtropics; present-day richness quantified using the typical cutoff of 23° would result in similar diversity in these regions.

We used two approaches to quantify macroevolutionary dynamics. In the first approach (Supplementary Fig. 37), we considered all site-by-age records, including those outside of 55° latitude. Speciation was considered to have occurred in the region of first occurrence for a species (Supplementary Fig. 39). Similarly, extinction was considered to have occurred in the region of last occurrence for a species. That is, even if a species was present in both temperate and tropical regions within a 2.5-Myr time bin, the species was counted as going extinct in the tropics if that region held the last occurrence. Extirpation was documented in the time bin when the species last disappeared from a region (either temperate or tropics) but persisted in the other region. In this way, each species had, at most, one extirpation. Dispersal dynamics were identified by documenting how long it took a species after origination to appear in a region different from where it originated; for example, if a species originated in the tropics, we assessed whether the species ever left the tropics, and, if so, how long it took the species to move to the temperate region. Species that originated and moved within a 2.5-Myr time bin were counted towards both metrics in that time bin. Raw counts (Supplementary Fig. 37), proportions (Supplementary Fig. 37) and per capita rates (Supplementary Fig. 40) were calculated.

In the second approach (Supplementary Fig. 38), we excluded species present in both temperate and tropical regions within a given 2.5-Myr time bin. These species do not contribute to the development of the LDG in our analyses. Thus, by focusing only on species present in one region, we can more clearly distinguish the processes contributing to LDG formation on the timescale of our analyses. For these analyses, we counted a speciation as the region of first occurrence for a species, but only if the species did not expand its range to another region in the same time bin. Extinction was recorded in the region where the species was last observed, but only if the species was found uniquely in that region. Extirpation occurred when a species was present in both regions but was lost from one region. Thus, extirpation could occur numerous times for each species over time, unlike in the previous approach. Dispersal was counted when a species moved from one region to another; for example, when a species was found only in the tropical region in one time bin to when it was found only in the temperate region in another time bin. The two approaches produced congruent conclusions, which is that low-latitude speciation and high-latitude regional extirpation contributed to the steepening of the diversity gradient over the past 40 Myr.

Incomplete sampling may affect the location of first and last appearances for taxa in the fossil record. Although it is unlikely that geographical error in the first and last appearances would be sufficient to mask true patterns given the broad geographical bins used here, we used a bootstrap resampling protocol to test this assumption. Each species was subsampled down to 75% of available records across its lifetime, and the evolutionary metrics (speciation, extinction, extirpation and dispersal) re-calculated for each time bin. This subsampling process was repeated 100 times, such that 100 temperate and 100 tropical estimates were returned for each metric (speciation, extinction, extirpation and dispersal) in each time bin. Our goal was to assess how sampling may affect understanding of the location of first and last appearance and dispersal patterns for species. The estimates, however, remained broadly consistent across bootstrap replicates (Supplementary Figs. 41–43), most probably because planktonic foraminifera are densely sampled with high spatiotemporal resolution—arguably the best of any fossil group⁵². Planktonic foraminifera are used extensively for biostratigraphy and have been subject to considerable taxonomic revision, resulting in well-established stratigraphic ranges⁸⁷; accordingly, the geographical locations of first and last occurrences in Triton that correlate with these datums are robust.

Reporting summary

Further information on research design is available in the Nature Portfolio Reporting Summary linked to this article.

Data availability

All data to reproduce our analyses are provided in <https://doi.org/10.6084/m9.figshare.21355467>. The spatiotemporal planktonic foraminiferal occurrence data were derived from Triton, an open-source database³².

Code availability

All code to reproduce the analyses is provided in <https://doi.org/10.6084/m9.figshare.21355467>. Our custom code relied on the following R packages: HHR package v.3.1-47, spatialreg R package v.1.2-3, geosphere R package, vegan R package v.2.5-7 and mapast R package v.0.1.

52. Aze, T. et al. A phylogeny of Cenozoic macroperforate planktonic foraminifera from fossil data. *Biol. Rev.* **86**, 900–927 (2011).
53. Matthews, K. J. et al. Global plate boundary evolution and kinematics since the late Paleozoic. *Glob. Planet. Change* **146**, 226–250 (2016).
54. Gyldefeldt, A.-B. V., Carstens, J. & Meincke, J. Estimation of the catchment area of a sediment trap by means of current meters and foraminiferal tests. *Deep Sea Res. Part II* **47**, 1701–1717 (2000).
55. Qiu, Z., Doglioli, A. M. & Carlotti, F. Using a Lagrangian model to estimate source regions of particles in sediment traps. *Sci. China Earth Sci.* **57**, 2447–2456 (2014).
56. Siegel, D. A. & Deuser, W. G. Trajectories of sinking particles in the Sargasso Sea: modeling of statistical funnels above deep-ocean sediment traps. *Deep Sea Res. Part I* **44**, 1519–1541 (1997).
57. Waniek, J., Koeve, W. & Prien, R. D. Trajectories of sinking particles and the catchment areas above sediment traps in the Northeast Atlantic. *J. Mar. Res.* **58**, 983–1006 (2000).
58. R Core Team. *R: A Language and Environment for Statistical Computing* <http://www.R-project.org> (R Foundation for Statistical Computing, 2019).
59. Alroy, J. The fossil record of North American mammals: evidence for a Paleocene evolutionary radiation. *Syst. Biol.* **48**, 107–118 (1999).
60. Marcot, J. D. The fossil record and macroevolutionary history of North American ungulate mammals: standardizing variation in intensity and geography of sampling. *Paleobiology* **40**, 238–255 (2014).
61. Gaston, K. J., Williams, P. H., Eggleton, P. & Humphries, C. J. Large scale patterns of biodiversity: spatial variation in family richness. *Proc. R. Soc. Lond. B* **260**, 149–154 (1995).
62. Valdes, P. J. et al. The BRIDGE HadCM3 family of climate models: HadCM3@Bristol v1.0. *Geosci. Model Dev.* **10**, 3715–3743 (2017).
63. Cox, P. M. et al. The impact of new land surface physics on the GCM simulation of climate and climate sensitivity. *Clim. Dyn.* **15**, 183–203 (1999).
64. Sagoo, N., Valdes, P., Flecker, R. & Gregoire, L. J. The Early Eocene equable climate problem: can perturbations of climate model parameters identify possible solutions? *Phil. Trans. R. Soc. A* **371**, 20130123 (2013).
65. Kiehl, J. T. & Shields, C. A. Sensitivity of the Palaeocene–Eocene thermal maximum climate to cloud properties. *Phil. Trans. R. Soc. A* **371**, 20130093 (2013).
66. Cox, M. D. *A Primitive Equation, 3-Dimensional Model of the Ocean*. GFDL Ocean Group Technical Report No. 1 (GFDL Princeton Univ., 1984).
67. Collins, M., Tett, S. F. B. & Cooper, C. The internal climate variability of HadCM3, a version of the Hadley Centre coupled model without flux adjustments. *Clim. Dyn.* **17**, 61–81 (2001).
68. Farnsworth, A. et al. Climate sensitivity on geological timescales controlled by nonlinear feedbacks and ocean circulation. *Geophys. Res. Lett.* **46**, 9880–9889 (2019).
69. Valdes, P. J., Scotese, C. R. & Lunt, D. J. Deep ocean temperatures through time. *Clim. Past* **17**, 1483–1506 (2021).
70. Farnsworth, A. et al. Past East Asian monsoon evolution controlled by paleogeography, not CO₂. *Sci. Adv.* **5**, eaax1697 (2019).
71. Jones, L. A., Mannion, P. D., Farnsworth, A., Bragg, F. & Lunt, D. J. Climatic and tectonic drivers shaped the tropical distribution of coral reefs. *Nat. Commun.* **13**, 3120 (2022).
72. Scotese, C. R. & Wright, N. PALEOMAP paleogeographic elevation models (PaleoDEMS) for the Phanerozoic. Zenodo <https://doi.org/10.5281/zenodo.5460860> (2018).
73. Foster, G. L., Royer, D. L. & Lunt, D. J. Future climate forcing potentially without precedent in the last 420 million years. *Nat. Commun.* **8**, 14845 (2017).
74. Gough, D. O. Solar interior structure and luminosity variations. *Sol. Phys.* **74**, 21–34 (1981).
75. Farnsworth, A. et al. Paleoclimate model-derived thermal lapse rates: towards increasing precision in paleoaltimetry studies. *Earth Planet. Sci. Lett.* **564**, 116903 (2021).
76. Bahcall, J. N., Pinsonneault, M. H. & Basu, S. Solar models: current epoch and time dependences, neutrinos, and helioseismological properties. *Astrophys. J.* **555**, 990–1012 (2001).
77. Hawkins, E. & Sutton, R. The potential to narrow uncertainty in regional climate predictions. *Bull. Am. Meteorol. Soc.* **90**, 1095–1108 (2009).
78. Kraus, E. B. & Turner, J. S. A one-dimensional model of the seasonal thermocline II. The general theory and its consequences. *Tellus* **19**, 98–105 (1967).

79. Foreman, S. J. *The Ocean Model Report*. Unified Model Documentaiton Paper Number 40 (The Met Office, 2005).
80. HH: Statistical Analysis and Data Display: Heiberger and Holland. R package version 3.1-47 (2022).
81. Zuur, A. F., Ieno, E. N. & Elphick, C. S. A protocol for data exploration to avoid common statistical problems. *Methods Ecol. Evol.* **1**, 3–14 (2010).
82. Bivand, R., Mollo, G. & Piras, G. A review of software for spatial econometrics in R. *Mathematics* **9**, 1276 (2021).
83. Benjamini, Y. & Hochberg, Y. Controlling the false discovery rate: a practical and powerful approach to multiple testing. *J. R. Stat. Soc.* **57**, 289–300 (1995).
84. Cooper, N. & Purvis, A. Body size evolution in mammals: complexity in tempo and mode. *Am. Nat.* **175**, 727–738 (2010).
85. geosphere: Spherical Trigonometry. R package version 1.5-14 (2021).
86. Oksanen, J. et al. vegan: Community Ecology Package. R package version 2.5-7 (2020).
87. Wade, B. S., Pearson, P. N., Berggren, W. A. & Pälike, H. Review and revision of Cenozoic tropical planktonic foraminiferal biostratigraphy and calibration to the geomagnetic polarity and astronomical time scale. *Earth Sci. Rev.* **104**, 111–142 (2011).

Acknowledgements We thank A. Woodhouse, G. Antell, P. Hull, H. Johnson, H. Bouman and W. Kiessling for informative discussions; we are grateful to Triton and Neptune database

contributors, from which Triton heavily draws. E.E.S. was supported by Leverhulme Trust grant RPG-201170, the Leverhulme Prize and the Natural Environment Research Council grant NE/V011405/1.

Author contributions E.E.S. conceptualized the study. E.E.S. and I.S.F. devised the methodology. I.S.F., E.E.S., A.F. and P.V. conducted the investigation. T.A., I.S.F. and E.E.S. performed visualization. E.E.S. acquired funding. E.E.S. conducted project administration. E.E.S. supervised the study. E.E.S. wrote the original draft of the manuscript. E.E.S., I.S.F., T.A., A.F. and P.V. reviewed and edited the manuscript.

Competing interests The authors declare no competing interests.

Additional information

Supplementary information The online version contains supplementary material available at <https://doi.org/10.1038/s41586-023-05712-6>.

Correspondence and requests for materials should be addressed to Erin E. Saupe.

Peer review information *Nature* thanks Moriaki Yasuhara and the other, anonymous, reviewer(s) for their contribution to the peer review of this work.

Reprints and permissions information is available at <http://www.nature.com/reprints>.

Reporting Summary

Nature Portfolio wishes to improve the reproducibility of the work that we publish. This form provides structure for consistency and transparency in reporting. For further information on Nature Portfolio policies, see our [Editorial Policies](#) and the [Editorial Policy Checklist](#).

Statistics

For all statistical analyses, confirm that the following items are present in the figure legend, table legend, main text, or Methods section.

n/a Confirmed

- ☒ ☐ The exact sample size (n) for each experimental group/condition, given as a discrete number and unit of measurement
- ☒ ☐ A statement on whether measurements were taken from distinct samples or whether the same sample was measured repeatedly
- ☒ ☐ The statistical test(s) used AND whether they are one- or two-sided
Only common tests should be described solely by name; describe more complex techniques in the Methods section.
- ☒ ☐ A description of all covariates tested
- ☒ ☐ A description of any assumptions or corrections, such as tests of normality and adjustment for multiple comparisons
- ☒ ☐ A full description of the statistical parameters including central tendency (e.g. means) or other basic estimates (e.g. regression coefficient) AND variation (e.g. standard deviation) or associated estimates of uncertainty (e.g. confidence intervals)
- ☒ ☐ For null hypothesis testing, the test statistic (e.g. F , t , r) with confidence intervals, effect sizes, degrees of freedom and P value noted
Give P values as exact values whenever suitable.
- ☒ ☐ For Bayesian analysis, information on the choice of priors and Markov chain Monte Carlo settings
- ☒ ☐ For hierarchical and complex designs, identification of the appropriate level for tests and full reporting of outcomes
- ☒ ☐ Estimates of effect sizes (e.g. Cohen's d , Pearson's r), indicating how they were calculated

Our web collection on [statistics for biologists](#) contains articles on many of the points above.

Software and code

Policy information about [availability of computer code](#)

Data collection No code was needed for data collection.

Data analysis All code was written in the R programming language. This code is provided at the following DOI: <https://doi.org/10.6084/m9.figshare.21355467>. The following R packages were included in the custom code provided in the above DOI link:
HH R package v. 3.1-47
spatialreg R package v.1.2-3
geosphere R package
vegan R package v.2.5-7
mapast R package v.0.1

For manuscripts utilizing custom algorithms or software that are central to the research but not yet described in published literature, software must be made available to editors and reviewers. We strongly encourage code deposition in a community repository (e.g. GitHub). See the Nature Portfolio [guidelines for submitting code & software](#) for further information.

Data

Policy information about [availability of data](#)

All manuscripts must include a [data availability statement](#). This statement should provide the following information, where applicable:

- Accession codes, unique identifiers, or web links for publicly available datasets
- A description of any restrictions on data availability
- For clinical datasets or third party data, please ensure that the statement adheres to our [policy](#)

All data to replicate these analyses are publicly available at the following DOI: <https://doi.org/10.6084/m9.figshare.21355467>. The specimen occurrence records derive from the Triton Database, which is freely available (Fenton et al. 2021. Scientific Data): <https://www.nature.com/articles/s41597-021-00942-7>. Climate data derive from the Bridge Model Group: <https://www.paleo.bristol.ac.uk/resources/simulations/>. Climatic values across space and through time needed to replicate our analyses are included in data package in the DOI link above.

Human research participants

Policy information about [studies involving human research participants and Sex and Gender in Research](#).

Reporting on sex and gender

N/A

Population characteristics

N/A

Recruitment

N/A

Ethics oversight

N/A

Note that full information on the approval of the study protocol must also be provided in the manuscript.

Field-specific reporting

Please select the one below that is the best fit for your research. If you are not sure, read the appropriate sections before making your selection.

- ☒ Life sciences ☐ Behavioural & social sciences ☐ Ecological, evolutionary & environmental sciences

For a reference copy of the document with all sections, see [nature.com/documents/nr-reporting-summary-flat.pdf](https://www.nature.com/documents/nr-reporting-summary-flat.pdf)

Life sciences study design

All studies must disclose on these points even when the disclosure is negative.

Sample size

We quantified temporal patterns in LDGs using 434,113 unique species-by-locality-by-age records from the Triton database. All data from Triton were used, unless deemed to have been subject to dissolution. Patterns were quantified both with and without sub-sampling. Details of our sub-sampling procedure are provided in section 1.3.1 of the methods.

Data exclusions

No data were excluded from our study, unless samples were deemed to have been subject to dissolution, which could distort understanding of species richness.

Replication

We analysed latitudinal diversity gradient patterns using five different approaches, in order to assess the sensitivity of our pattern to methodological choice. All replication methods were successful, and details are provided in the methods.

Randomization

We employed subsampling to estimate diversity using bootstrap replicates, detailed in the methods.

Blinding

Blinding was not relevant to this study, since no human subjects were involved.

Reporting for specific materials, systems and methods

We require information from authors about some types of materials, experimental systems and methods used in many studies. Here, indicate whether each material, system or method listed is relevant to your study. If you are not sure if a list item applies to your research, read the appropriate section before selecting a response.

Materials & experimental systems

- n/a Involved in the study
- ☒ ☐ Antibodies
- ☒ ☐ Eukaryotic cell lines
- ☐ ☒ Palaeontology and archaeology
- ☒ ☐ Animals and other organisms
- ☒ ☐ Clinical data
- ☒ ☐ Dual use research of concern

Methods

- n/a Involved in the study
- ☒ ☐ ChIP-seq
- ☒ ☐ Flow cytometry
- ☒ ☐ MRI-based neuroimaging

Palaeontology and Archaeology

Specimen provenance	We quantified temporal patterns in LDGs using 434,113 unique species-by-locality-by-age records from the Triton database. Specimen locality information in Triton was derived primarily from ocean drilling projects over the last two decades. Planktonic foraminifera are single-celled protists that live in the open ocean.
Specimen deposition	All data can be accessed through the code and materials provided with this paper (https://doi.org/10.6084/m9.figshare.21355467), and through the open access database, Triton (Fenton et al. 2021 Scientific Data): https://www.nature.com/articles/s41597-021-00942-7
Dating methods	No new dates were obtained in this study. Ages of samples were taken from the Triton database (Fenton et al. 2021 Scientific Data): https://www.nature.com/articles/s41597-021-00942-7 .
<input checked="" type="checkbox"/> Tick this box to confirm that the raw and calibrated dates are available in the paper or in Supplementary Information.	
Ethics oversight	None.

Note that full information on the approval of the study protocol must also be provided in the manuscript.